Ferromagnetic Eu2+-based oxide glasses with reentrant spin glass behavior

AUTHOR(S):

Akamatsu, Hirofumi; Fujita, Koji; Murai, Shunsuke; Tanaka, Katsuhisa

CITATION:

Akamatsu, Hirofumi ...[et al]. Ferromagnetic Eu2+-based oxide glasses with reentrant spin glass behavior. PHYSICAL REVIEW B 2010, 81(1): 014423.

ISSUE DATE:

2010

URL:

http://hdl.handle.net/2433/148376

PHYSICAL REVIEW B **81**, 014423 (2010)

Ferromagnetic Eu^{2+}-based oxide glasses with reentrant spin glass behavior

Hirofumi Akamatsu, Koji Fujita,* Shunsuke Murai, and Katsuhisa Tanaka
Department of Material Chemistry, Graduate School of Engineering, Kyoto University, Nishikyo-ku, Kyoto 615-8510, Japan
(Received 13 October 2009; revised manuscript received 4 January 2010; published 29 January 2010)

In most amorphous insulating magnets, the magnetic structure is dominated by the random distribution of magnetic moments as well as the predominant antiferromagnetic interaction among them, inevitably leading to a transition from high-temperature paramagnetic to low-temperature spin glass phase. In this paper, we report our discovery of *ferromagnetic* amorphous oxides with reentrant spin glass behavior. Unlike most oxide glasses, there is a strong tendency for the magnetic interaction of Eu^{2+} ions to be ferromagnetic in oxide glasses, as obviously indicated by the positive values of Weiss temperature. Comprehensive investigations of low-temperature magnetic properties for the present Eu^{2+}-containing glasses have revealed a typical behavior of reentrant ferromagnets. We discuss the possible mechanisms behind the ferromagnetic interactions, as well as the origin of reentrant spin glass nature, based on the specific electronic structure of Eu^{2+} compounds.

DOI: 10.1103/PhysRevB.81.014423 PACS number(s): 75.50.Kj, 75.10.Nr, 75.50.Lk

I. INTRODUCTION

A. Magnetic properties of amorphous insulators

Amorphous oxide magnets, where the magnetic cations are randomly distributed in the three-dimensional disordered network, have attracted attention as an example of an insulating spin glass (SG). Due to the insulating properties, their magnetic properties are dominated by so-called short-range superexchange interactions via oxide ions in contrast to canonical SGs, where the long-range Ruderman-Kittel-Kasuya-Yoshida interactions via conduction electrons play an important role in the SG ordering.[1] This type of superexchange interaction was first proposed by Kramers[2] and systematized by Anderson.[3] According to the Kanamori-Goodenough rule, which refines Kramers-Anderson (KA) mechanism so that this rule can be applied to various transition-metal oxides, the sign and strength of superexchange interactions depend on the sorts of transition-metal ions and the angle of *M*-O-*M* bonds where *M* is the transition metal and O is oxygen in insulating oxides.[4,5] In most cases, the nature of superexchange interactions between two identical *M* ions changes from strong antiferromagnetic (AFM) to weak ferromagnetic (FM) ones when the *M*-O-*M* angle is varied from 180° to 90°.[4,5] Therefore, the sign of superexchange interaction, as well as its strength, can have a wide distribution in amorphous oxides. Nonetheless, in most magnetic oxide glasses containing 3*d* transition-metal ions, AFM interactions are dominant over FM interactions, as experimentally indicated by the negative Weiss temperature (θ_W).[6–12] This also holds for oxide glasses containing rare-earth ions.[13,14] These facts reflect the open structure of glasses; magnetic oxide glasses favor the AFM interactions characteristic of 180° *M*-O-*M* bond. The situation that the magnetic moments are spatially distributed at random makes it impossible to realize that all the pairs of magnetic moments are completely coupled in an antiparallel way. Consequently, the random distribution of magnetic ions and the prevailing AFM interactions among them inevitably cause geometrical frustration in the arrangement of magnetic moments, leading to the SG transitions in magnetic oxide glasses. Actually, most oxide glasses containing a large number of transition-metal ions exhibit paramagnetic (PM)-SG transitions at low temperatures of several Kelvins.[6–12,15–17]

B. Rare examples of amorphous insulators with FM interactions

There exist very few reports concerning amorphous insulating compounds with positive values of θ_W, i.e., amorphous insulators in which FM rather than AFM interactions are predominant.[18,19] Litterst[18] found that a noncrystalline FeF_2 film prepared by a molecular-beam condensation had $\theta_W = +22$ K, in contrast to $\theta_W = -117$ K (Ref. 20) in the crystalline counterpart that is an antiferromagnet with $T_N = 78$ K.[21] It was proposed that the superexchange for configuration of nearly 90° Fe^{2+}-F^--Fe^{2+} angle might be an origin of the FM interactions although no clear explanation was given to confirm the prevalence of 90° Fe^{2+}-F^--Fe^{2+} bonds. Litterst also interpreted the unusual magnetic properties in terms of superparamagnetism of ultrafine FM particles; however, no experimental evidences were presented to convince the presence of the particles. Thus, the origin of FM interactions and the magnetically ordered phase remain uncovered. Also, it should be noted that the FM properties depended on the substrate temperature during the film deposition; namely, the FM properties could not be observed for the noncrystalline FeF_2 film prepared under a different deposition condition. In addition, it was reported in some literatures that other amorphous insulators containing Fe^{2+} ions prefer AFM rather than FM interactions.[6,7] These results mean that FM interactions are not always predominant among Fe^{2+} ions in the disordered lattice.

Another curious example was shown by Schoenes *et al.*,[19] who reported that a positive value of $\theta_W(=+1$ K) was obtained for binary europium silicate glass with $Eu^{2+}_{0.12}Eu^{3+}_{0.02}Si_{0.31}O_{0.55}$ composition in which Eu^{2+} ions accounted for 27 mol % of the whole cations. Nevertheless, no magnetic transition was observed down to 1.5 K, which was the lowest measurement temperature, in the europium silicate glass. Despite their fascinating discovery, the magnetic properties of Eu^{2+}-containing oxide glasses have been scarcely investigated since then. Recently, Sugihara *et al.*[22] studied the magnetic properties of oxide glasses with nominal compositions of $50EuAl_2O_4 \cdot 50B_2O_3$ and $50EuAl_2O_4 \cdot 10B_2O_3 \cdot 40SiO_2$, where the molar ratio of Eu^{2+} to the total europium ion, $f_{Eu^{2+}}$, was estimated to be 0.024

and 0.174, respectively. In this case, however, it is naturally anticipated that a large number of Eu^{3+} ions remaining in the glasses brings about the Van Vleck paramagnetism, which hampers observation of the magnetic behavior inherent in Eu^{2+} ions. The preparation of glasses with high $f_{Eu^{2+}}$ is, therefore, necessary for evaluating the intrinsic magnetic behavior of Eu^{2+} in amorphous oxides.

Here, three questions remain to be solved for magnetic properties of Eu^{2+}-based oxide glasses: (i) whether the FM interaction rather than the AFM one is commonly predominant among Eu^{2+} ions dispersed homogeneously in any oxide glass matrix, (ii) what the origin of the FM interaction is, and (iii) what kind of magnetically ordered phase appears at low temperatures, especially when high concentrations of Eu^{2+} ions are incorporated into glasses. In particular, the last question is fascinating from a viewpoint of whether a long-range FM order is realized in an insulator with a completely disordered lattice.

C. Outline

In the present paper, in order to address the above-mentioned questions, we have prepared bulk oxide glasses with high concentrations of Eu^{2+} ions ranging from 10.9 to 45.3 mol % (see Table III), and carried out comprehensive examination of their magnetic properties. The experimental procedures are depicted in Sec. II. The structural characterization of the glasses is described in Sec. III. The amorphous nature and homogeneity of the glasses are confirmed by x-ray diffraction (XRD) and transmission electron microscopy (TEM). The valence state of europium ions and local structure of Eu^{2+} ions are investigated by ^{151}Eu Mössbauer effect measurements. We present the magnetic properties in Sec. IV. Our results indicate that θ_W is positive irrespective of glass composition and becomes higher with increasing Eu^{2+} concentration, suggesting that the prevalence of FM interaction is a common characteristic of oxide glasses containing Eu^{2+} ions. We also demonstrate that the low-temperature magnetic behavior of the present glasses manifests remarkable similarities to the transitions of reentrant ferromagnets. In Sec. V, possible mechanisms of the observed FM interactions are discussed on the basis of FM exchange mechanisms proposed for Eu^{2+}-based crystalline materials.[23,24] The conclusions are summarized in Sec. VI.

II. EXPERIMENTAL PROCEDURE

We have studied EuO-B_2O_3, EuO-Al_2O_3-B_2O_3, and EuO-Al_2O_3-SiO_2-B_2O_3 glass systems because of their broad glass-forming regions extended into EuO-rich compositions. The glass compositions and their notations are listed in Table I. The detail of glass preparation is as follows. First, reagent grade Eu_2O_3, B_2O_3, Al_2O_3, and SiO_2 were weighed to obtain the prescribed compositions and mixed thoroughly in an alumina mortar. The mixture was then melted in a glassy carbon crucible or a graphite crucible for 30–120 min in an Ar(95)/H_2(5) (vol. %) atmosphere at 1400–1500 °C so that Eu^{3+} ions were reduced into Eu^{2+} ions. The melt in a crucible was cooled to room temperature in an N_2 atmosphere. The conditions of glass melting are also shown in Table I. For the resultant glasses, we performed XRD measurements using Cu $K\alpha$ radiation (RINT2500, Rigaku) and TEM observation with selected area electron diffraction (SAED) (JEM-2100F, JEOL).

TABLE I. Glass compositions and their notations. The conditions of glass melting are also shown.

Notation	Composition (mol %)	Condition (°C, min)
25EuB1	$25.0EuO \cdot 75.0B_2O_3$	1400, 30[a]
25EuB2	$25.0EuO \cdot 75.0B_2O_3$	1400, 60[b]
30EuB1	$30.0EuO \cdot 70.0B_2O_3$	1400, 30[a]
30EuB2	$30.0EuO \cdot 70.0B_2O_3$	1400, 60[b]
40EuAlB	$40.0EuO \cdot 10.0Al_2O_3 \cdot 50.0B_2O_3$	1450, 30[a]
50EuAlB1	$50.0EuO \cdot 10.0Al_2O_3 \cdot 40.0B_2O_3$	1450, 30[a]
50EuAlB2	$50.0EuO \cdot 10.0Al_2O_3 \cdot 40.0B_2O_3$	1450, 30[b]
50EuAlB3	$50.0EuO \cdot 10.0Al_2O_3 \cdot 40.0B_2O_3$	1450, 60[b]
50EuAlB4	$50.0EuO \cdot 20.0Al_2O_3 \cdot 30.0B_2O_3$	1500, 30[b]
53EuAlB	$52.5EuO \cdot 10.0Al_2O_3 \cdot 37.5B_2O_3$	1500, 60[b]
47EuAlBSi	$46.7EuO \cdot 13.3Al_2O_3 \cdot 13.3B_2O_3 \cdot 26.7SiO_2$	1500, 60[b]
50EuAlBSi	$50.0EuO \cdot 12.5Al_2O_3 \cdot 17.5B_2O_3 \cdot 20.0SiO_2$	1500, 60[b]
55EuAlBSi	$55.0EuO \cdot 10.0Al_2O_3 \cdot 15.0B_2O_3 \cdot 20.0SiO_2$	1500, 60[b]
58EuAlBSi1	$58.0EuO \cdot 12.0Al_2O_3 \cdot 20.0B_2O_3 \cdot 10.0SiO_2$	1500, 60[b]
58EuAlBSi2	$58.0EuO \cdot 12.0Al_2O_3 \cdot 20.0B_2O_3 \cdot 10.0SiO_2$	1450, 120[b]
58EuAlBSi3	$58.0EuO \cdot 12.0Al_2O_3 \cdot 20.0B_2O_3 \cdot 10.0SiO_2$	1500, 120[b]
59EuAlBSi	$59.0EuO \cdot 11.0Al_2O_3 \cdot 20.0B_2O_3 \cdot 10.0SiO_2$	1500, 120[b]
60EuAlBSi	$60.0EuO \cdot 11.0Al_2O_3 \cdot 19.5B_2O_3 \cdot 9.5SiO_2$	1500, 120[b]

[a]Melting in a glassy carbon crucible.
[b]Melting in a graphite crucible.

^{151}Eu Mössbauer effect measurements were performed at room temperature using 1.85 GBq $^{151}Sm_2O_3$ as a 21.5 keV γ-ray source. The details of experiments were described in Ref. 25. The velocity calibration was done with the magnetic hyperfine spectrum of α-Fe foil obtained using a 14.4 keV γ ray of ^{57}Co doped in Rh. The Mössbauer spectrum of EuF_3 was utilized as a standard for isomer shift (IS). The magnetic measurements were performed by a superconducting quantum interference device magnetometer (MPMS XL, Quantum Design). Specific heat was measured at zero magnetic field by a heat-pulse relaxation method using a commercial calorimeter (PPMS, Quantum Design).

III. STRUCTURAL CHARACTERIZATION

A. XRD analysis and TEM observation

All of the glasses used in this study were identified to be amorphous by XRD analysis. The typical XRD patterns are displayed in Fig. 1(a) for $30.0EuO \cdot 70.0B_2O_3$, $52.5EuO \cdot 10.0Al_2O_3 \cdot 37.5B_2O_3$, and $60.0EuO \cdot 11.0Al_2O_3 \cdot 19.5B_2O_3 \cdot 9.5SiO_2$ glasses. No diffraction peaks attributable to any crystalline phases are detected; instead, halo patterns typical of amorphous structure are observed. Similar halo patterns were observed

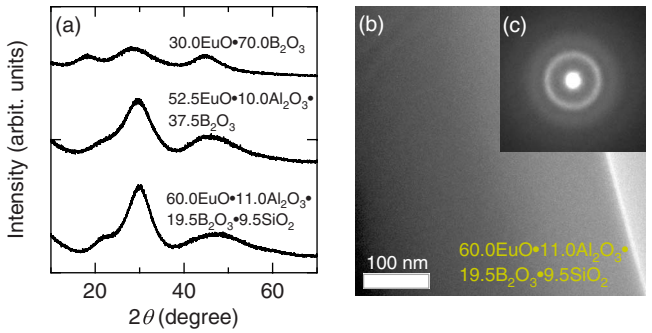

FIG. 1. (Color online) (a) XRD patterns of $30.0EuO \cdot 70.0B_2O_3$ (30EuB2), $52.5EuO \cdot 10.0Al_2O_3 \cdot 37.5B_2O_3$ (53EuAlB), and $60.0EuO \cdot 11.0Al_2O_3 \cdot 19.5B_2O_3 \cdot 9.5SiO_2$ (60EuAlBSi) glasses. (b) TEM image and (c) SAED of $60.0EuO \cdot 11.0Al_2O_3 \cdot 19.5B_2O_3 \cdot 9.5SiO_2$ glass.

for the other glasses as well. The amorphous nature of $60.0EuO \cdot 11.0Al_2O_3 \cdot 19.5B_2O_3 \cdot 9.5SiO_2$ glass is also corroborated by high-resolution TEM image [Fig. 1(b)] and SAED pattern [Fig. 1(c)], clearly indicating that the glass can be formed without inhomogeneity such as precipitation of crystals or phase separation.

B. ^{151}Eu Mössbauer spectroscopy

Figure 2(a) displays Mössbauer spectra for $30.0EuO \cdot 70.0B_2O_3$, $52.5EuO \cdot 10.0Al_2O_3 \cdot 37.5B_2O_3$, and $60.0EuO \cdot 11.0Al_2O_3 \cdot 19.5B_2O_3 \cdot 9.5SiO_2$ glasses. Each of the spectra is composed of two absorption peaks at about −13 mm/s and 0 mm/s, ascribed to Eu^{2+} and Eu^{3+} ions, respectively. The fraction of absorption area of Eu^{2+} ion is larger than 90%, implying that at least 90% of Eu ions are present as the divalent state in these glasses.[26] The single, slightly asymmetric and broad line due to Eu^{2+} results from the unresolved quadrupole interaction;[25] thus, we analyzed

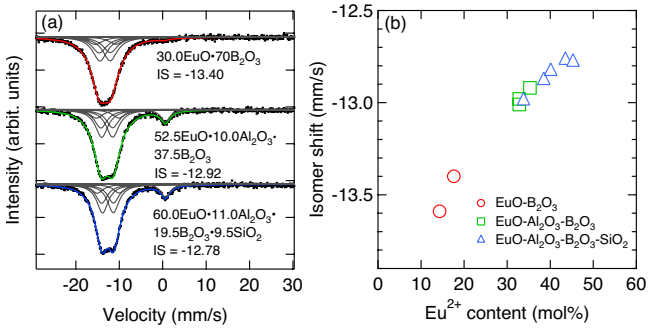

FIG. 2. (Color online) (a) ^{151}Eu Mössbauer spectra of $30.0EuO \cdot 70.0B_2O_3$ (30EuB2), $52.5EuO \cdot 10.0Al_2O_3 \cdot 37.5B_2O_3$ (53EuAlB), and $60.0EuO \cdot 11.0Al_2O_3 \cdot 19.5B_2O_3 \cdot 9.5SiO_2$ (60EuAlBSi) glasses at room temperature. The values of IS are also shown. The calculated spectra are drawn as solid curves. (b) Relationship between the IS value and Eu^{2+} concentration: 25EuB2, 30EuB2 (red open circles), 50EuAlB3, 50EuAlB4, 53EuAlB (green open squares), 47EuAlBSi, 55EuAlBSi, 58EuAlBSi2, 59EuAlBSi, and 60EuAlBSi (blue open triangle). For the abbreviation of notation, see Table I.

TABLE II. Mössbauer parameters obtained by the fit of theoretical curve to the experimental spectrum.

Notation	δ[a] (mm/s)	γ[b] (mm/s)	eQ_gV_{zz}[c] (mm/s)	η[d]
25EuB2	−13.59	4.58	−13.32	1.00
30EuB2	−13.40	4.14	−14.43	0.91
50EuAlB3	−12.98	3.21	−14.07	0.98
50EuAlB4	−13.01	3.91	−16.18	1.00
53EuAlB	−12.92	3.61	−15.28	0.95
47EuAlBSi	−12.99	3.94	−16.26	1.00
55EuAlBSi	−12.88	3.14	−14.37	0.97
58EuAlBSi2	−12.83	3.38	−14.82	0.96
59EuAlBSi	−12.76	3.37	−14.73	1.00
60EuAlBSi	−12.78	3.29	−14.95	0.97

[a] δ: isomer shift relative to EuF_3.
[b] γ: FWHM of one component of Lorentzian multiples.
[c] eQ_gV_{zz}: quadrupole interaction parameter.
[d] η: asymmetry parameter.

the Eu^{2+} absorption line using multiplet components of Lorentzian shape, corresponding to 12 transitions between ground state (nuclear spin $I=I_g=5/2$, quadrupole moment $Q=Q_g$) and excited state ($I=I_e=7/2, Q=Q_e$). The analyses were made using the method for a pure quadrupole spectrum proposed by Shenoy and Dunlap,[27] with $Q_e/Q_g=1.34$.[23,25] By contrast, a single Lorentzian was used to reproduce the Eu^{3+} absorption line because of the poor spectral resolution. By fitting the theoretical spectra [the solid lines in Fig. 2(a)] to the experimental spectra, we obtained Mössbauer parameters. i.e., isomer shift (IS$=\delta$), quadrupole interaction parameter (QI$=eQ_gV_{zz}$), and asymmetric parameter ($\eta=(V_{yy}-V_{xx})/V_{zz}$), where V_{ll} is the electric field gradient in the direction l. The analysis gives $\delta=-13.40$ mm/s, $eQ_gV_{zz}=-14.43$ mm/s, and $\eta=0.91$ for $30.0EuO \cdot 70.0B_2O_3$ glass, $\delta=-12.92$ mm/s, $eQ_gV_{zz}=-15.28$ mm/s, and $\eta=0.95$ for $52.5EuO \cdot 10.0Al_2O_3 \cdot 37.5B_2O_3$ glass, and $\delta=-12.78$ mm/s, $eQ_gV_{zz}=-14.95$ mm/s, and $\eta=0.97$ for $60.0EuO \cdot 11.0Al_2O_3 \cdot 19.5B_2O_3 \cdot 9.5SiO_2$ glass. Table II summarizes the Mössbauer parameters for all of the glasses. The IS reflects the electron density at the nucleus, and in the present case, is a measure of the covalency of Eu^{2+}-O bond and/or the coordination number of oxide ion for Eu^{2+}.[25] The IS values for Eu^{2+} ions in the present glasses are comparable to those of perovskite-type oxides $EuTiO_3$ (−12.5 mm/s) and $EuZrO_3$ (−13.1 mm/s),[25] indicating that the average coordination number for Eu^{2+} ion is about 12. The variation in IS value with Eu^{2+} concentration is shown in Fig. 2(b). The IS value tends to increase with increasing the Eu^{2+} concentration, implying that the glasses with higher Eu^{2+} concentration have more covalent Eu^{2+}-O bonds. Furthermore, the density of states of bands consisting of Eu 5*d*, Eu 6*s*, and O 2*p* states has a broader width with an increase in the covalency of Eu^{2+}-O bonds, resulting in a decrease in the excitation energy from Eu 4*f* to 5*d* bands, U_{fd}. Actually, Tanaka *et al.* reported that in Eu^{2+}-containing oxide glasses the effective wavelength of transition from Eu 4*f* to 5*d*

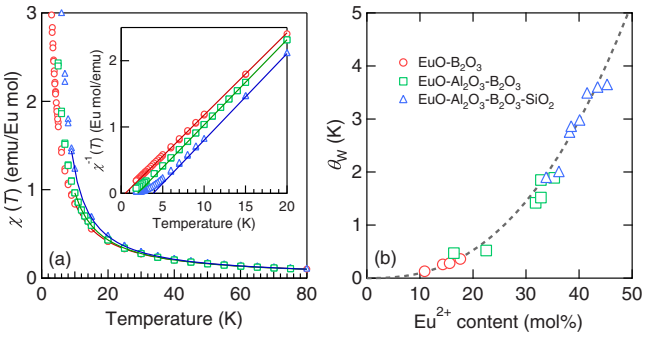

FIG. 3. (Color online) (a) Temperature dependence of magnetic susceptibility, $\chi(T)$, of $30.0EuO\cdot70.0B_2O_3$ (30EuB2, red circle), $52.5EuO\cdot10.0Al_2O_3\cdot37.5B_2O_3$ (53EuAlB, green square), and $60.0EuO\cdot11.0Al_2O_3\cdot19.5B_2O_3\cdot9.5SiO_2$ (60EuAlBSi, blue triangle) glasses. The solid curve represents the fit of Eq. (1) to the experimental data. The inset shows temperature dependence of inverse magnetic susceptibility, $\chi^{-1}(T)$, of the present glasses. The solid lines in the inset represent the fit of Curie-Weiss law to the experimental data in high-temperature region. (b) The Weiss temperature, θ_W, is plotted against the concentration of Eu^{2+} ion. The dashed curve is a guide to eyes.

bands, which led to Faraday effect, became longer when the IS value was larger.[28,29] On the other hand, the QI of Eu^{2+} reflects the electric field gradient caused by the surrounding ligands because zero orbital angular momentum resulting from the Eu^{2+} with $^8S_{7/2}$ ground state leads to no valence contribution.[25] The nonzero QI parameters, as well as nonzero η values, indicate the deviation from cubic symmetry and the absence of axial symmetry for coordination structure around Eu^{2+}.

IV. MAGNETIC PROPERTIES

A. High-temperature magnetic properties: Weiss temperature

Figure 3(a) depicts the dc magnetic susceptibility χ as a function of temperature T for $30.0EuO\cdot70.0B_2O_3$, $52.5EuO\cdot10.0Al_2O_3\cdot37.5B_2O_3$, and $60.0EuO\cdot11.0Al_2O_319.5B_2O_3\cdot9.5SiO_2$ glasses. The corresponding $\chi^{-1}(T)$ curves are displayed in the inset of Fig. 3(a). Both zero-field cooling (ZFC) and field cooling (FC) processes were carried out using a magnetic field of 50 Oe. The linear relationship in the temperature dependence of $\chi^{-1}(T)$ above 10 K reveals that the glasses are PM in the temperature range; the linear part is describable in terms of the Curie-Weiss law: $\chi^{-1}=(3k_B/N_A{M_B}^2{\mu_B}^2)(T-\theta_W)$, where N_A is the Avogadro constant, μ_B the Bohr magneton, M_B the effective number of Bohr magnetons, k_B the Boltzmann constant, and θ_W the Weiss temperature. The intercept of the solid lines in the inset of Fig. 3(a) is found to be positive for the present glasses, clearly indicating that FM interactions rather than AFM ones are dominant among Eu^{2+} spins. The upward deviation of $\chi^{-1}(T)$ curves from the Curie-Weiss law, as observed at temperatures below 10 K, is indicative of the emergence of short-range FM correlation at low temperatures. We have performed more rigorous analysis of susceptibility data by considering the contribution from the remaining Eu^{3+} ions, which are nonmagnetic in their ground state $^7F_0$ but have net moments in the excited states ^7F_J ($J=1,2,\ldots,6$). The susceptibility including contributions from Eu^{2+} and Eu^{3+} is expressed as

$$\chi(T)=f_{Eu^{2+}}\times\frac{N_A(7.94\mu_B)^2}{3k_B(T-\theta_W)}+(1-f_{Eu^{2+}})\times\frac{N_A\sum_{J=0}^{2}(2J+1)\exp(-E_J/k_BT)\left\{\frac{g_J{\mu_B}^2J(J+1)}{3k_BT}+\alpha_J\right\}}{\sum_{J=0}^{2}(2J+1)\exp(-E_J/k_BT)}. \quad (1)$$

where $f_{Eu^{2+}}$ is the molar ratio of Eu^{2+} to the total europium ion. The first term of Eq. (1) represents the Curie-Weiss paramagnetism of Eu^{2+}, and the second one includes the Curie paramagnetism of the excited states of Eu^{3+} and the Van Vleck paramagnetism of Eu^{3+}.[30] In the second term, g_J, E_J, and α_J are the g factor, the energy, and the Van Vleck magnetic susceptibility of the excited states $^7F_J(J=1,2,\ldots,6)$, respectively. For $J>0$, the energy difference between the J and $J-1$ states is given by $E_J-E_{J-1}=\lambda J$, where λ is the spin-orbital coupling constant. For Eu^{3+}, λ varies in a range of 320–370 cm^{-1} depending on the screening effect and crystal-field anisotropy.[31] In this analysis, we use $\lambda=348$ cm^{-1}, which is attained for EuB_3O_6 crystal.[31] Fits of Eq. (1) to the $\chi(T)$ curves in the high-temperature range (10–350 K) [see Fig. 3(a)] gives $\theta_W=0.36$ K and $f_{Eu^{2+}}=1.00$ for $30.0EuO\cdot70.0B_2O_3$ glass, $\theta_W=1.89$ K and $f_{Eu^{2+}}=0.99$ for $52.5EuO\cdot10.0Al_2O_3\cdot37.5B_2O_3$ glass, and $\theta_W=3.62$ K and $f_{Eu^{2+}}=0.98$ for $60.0EuO\cdot11.0Al_2O_3\cdot19.5B_2O_3\cdot9.5SiO_2$ glass. In Table III the values of $f_{Eu^{2+}}$ and θ_W obtained for the other glasses are presented. Table III also lists the nominal Eu ion concentration [Eu] and the calculated Eu^{2+} concentration [Eu^{2+}]. Here, [Eu] corresponds to the molar fraction of Eu ion relative to the total cation in the starting composition while [Eu^{2+}] can be evaluated by multiplying [Eu] by $f_{Eu^{2+}}$. It should be noted that the resultant $f_{Eu^{2+}}$ values are in agreement with those estimated from the fraction of Eu^{2+} absorption peak in Mössbauer spectra. The positive values of θ_W clearly indicate the prevalence of FM interactions among Eu^{2+} ions. This behavior is in contrast to experimental results as observed for many oxide glasses containing other magnetic ions such as $3d$ transition-metal and trivalent rare-earth ions, where AFM interaction is dominant.[6–14] In Fig. 3(b), θ_W is plotted against [Eu^{2+}]. As the Eu^{2+} concentration is increased from 10.9 to 45.3 mol %, the θ_W value monotonically increases from 0.13 to 3.62 K. In the molecular-field approximation, θ_W is represented as $J_{eff}N{M_B}^2$, where J_{eff} is the effective exchange integral and N the Eu^{2+} concentration. The value of θ_W increases with an increase in Eu^{2+} concentration more rapidly than the linear dependence, implying that J_{eff} becomes larger as the Eu^{2+} concentration increases.

B. Low-temperature magnetic properties: reentrant ferromagnet

Let us now turn our attention to the low-temperature magnetic properties of the glass with the highest Eu^{2+} concentra-

TABLE III. Nominal Eu ion concentration, [Eu], calculated Eu^{2+} concentration, [Eu^{2+}], molar ratio of Eu^{2+} to the total europium ion, $f_{Eu^{2+}}$, and Weiss temperature, θ_W.

Notation	[Eu] (mol %)	[Eu^{2+}][a] (mol %)	$f_{Eu^{2+}}$[b]	θ_W[b] (K)
25EuB1	14.3	10.9	0.73	0.13
25EuB2	14.3	14.3	1.00	0.26
30EuB1	17.6	15.6	0.89	0.28
30EuB2	17.6	17.6	1.00	0.36
40EuAlB	25.0	16.4	0.66	0.47
50EuAlB1	33.3	22.5	0.67	0.52
50EuAlB2	33.3	31.8	0.95	1.42
50EuAlB3	33.3	32.8	0.98	1.85
50EuAlB4	33.3	32.8	0.98	1.52
53EuAlB	35.6	35.3	0.99	1.89
47EuAlBSi	36.9	33.8	0.92	1.87
50EuAlBSi	38.5	36.2	0.94	1.98
55EuAlBSi	44.0	38.5	0.88	2.83
58EuAlBSi1	43.9	38.2	0.87	2.72
58EuAlBSi2	43.9	40.1	0.91	2.95
58EuAlBSi3	43.9	41.5	0.94	3.46
59EuAlBSi	45.0	43.5	0.97	3.57
60EuAlBSi	46.0	45.3	0.98	3.62

[a]The concentration [Eu^{2+}] was evaluated by multiplying [Eu] by $f_{Eu^{2+}}$.
[b]The values of $f_{Eu^{2+}}$ and θ_W were obtained by fitting the Eq. (1) to the $\chi(T)$ curves.

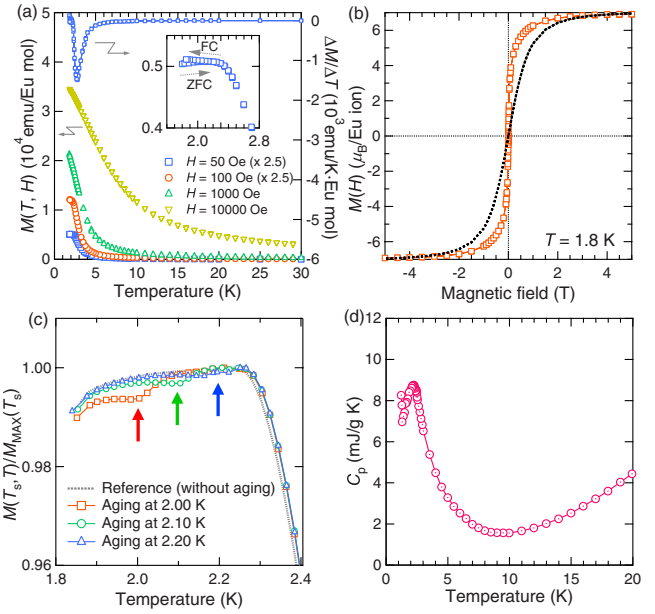

FIG. 4. (Color online) (a) Temperature dependence of magnetization, $M(T,H)$, measured in a magnetic field of 50, 100, 1000, and 10 000 Oe for $60.0EuO \cdot 11.0Al_2O_3 \cdot 19.5B_2O_3 \cdot 9.5SiO_2$ glass. Temperature derivative of $M(T,50\ \text{Oe})$ is also shown. The inset shows an enlarged view of $M(T,50\ \text{Oe})$ curve in low-temperature region. (b) Magnetic field dependence of magnetization, $M(H)$, measured at 1.8 K along with theoretical magnetization curve for a free Eu^{2+} ion at 1.8 K calculated using a Brillouin function (broken line). (c) Zero-field memory effect observed by applying a protocol proposed by Mathieu *et al.* (Ref. 36). $M(T_s,T)/M_{MAX}(T_s)$ curves are displayed for T_s=2.00, 2.10, and 2.20 K, where $M_{MAX}(T_s)$ is the maximum value of $M(T_s,T)$. (d) Specific heat, C_p, as a function of temperature.

tion, i.e., $60.0EuO \cdot 11.0Al_2O_3 \cdot 19.5B_2O_3 \cdot 9.5SiO_2$ glass. Figure 4(a) presents the temperature dependence of magnetization, $M(T,H)$, measured in magnetic fields of 50, 100, 1000, and 10 000 Oe, and the temperature derivative of $M(T,50\ \text{Oe})$ in a temperature range of 1.8–30 K. Below 3 K, $M(T,50\ \text{Oe})$ increases steeply with decreasing the temperature and exhibits an inflection point between 2.5 and 3.0 K, indicating the signature of FM transition. Figure 4(b) depicts the field dependence of magnetization, $M(H)$, measured at 1.8 K along with the theoretical magnetization curve for a free Eu^{2+} ion (S=7/2) at 1.8 K calculated using a Brillouin function. In the low-field region, the experimental $M(H)$ curve increases more steeply than the theoretical one with increasing the magnetic field, reflecting a strong tendency for Eu^{2+} spins to align ferromagnetically. In the high-field region, the saturated magnetization per Eu ion reaches $7\mu_B$, in good agreement with the theoretical spin-only magnetic moment of Eu^{2+}. This result also coincides with the fact that almost all the europium ions are present as Eu^{2+}, as revealed by the analyses of the ^{151}Eu Mössbauer spectra and the temperature dependence of susceptibility. The $M(H)$ curve demonstrates a very small magnetic hysteresis characteristic of soft ferromagnets. The soft FM behavior was observed in other Eu^{2+}-based magnets as well.[32,33] The inset of Fig. 4(a) illustrates an enlarged view of $M(T,50\ \text{Oe})$ curves in the low-temperature region. Both the FC and ZFC curves exhibit a plateaulike behavior below about 2.2 K. A close look at the figure reveals a slight discrepancy between FC and ZFC curves below about 2.2 K, which is characteristic of frustrated magnets such as SG. Even in a relatively low magnetic field such as 1000 Oe, the plateaulike behavior and the discrepancy between FC and ZFC curves disappear in the temperature dependence of magnetization because of the high sensitivity to the magnetic field. These features are reminiscent of ferromagnets with reentrant SG (RSG) nature.[34,35]

Zero-field cooling memory effects have been examined to confirm the SG nature of $60.0EuO \cdot 11.0Al_2O_3 \cdot 19.5B_2O_3 \cdot 9.5SiO_2$ glass. The experiments have been performed using the protocol proposed by Mathieu *et al.*[36] as follows. First, the present glass sample was cooled at a rate of 0.02 K/min from 2.4 K, at which the present glass is paramagnetic, to a stopping temperature T_s =2.00, 2.10, and 2.20 K. After aging at T_s for 3 h, the glass sample was recooled to 1.85 K at a rate of 0.02 K/min. Subsequently, a magnetic field of 1 Oe was applied and $M(T_s,T)$ was measured on heating at a rate of 0.02 K/min.[37] As a reference, $M(\text{ref},T)$ was determined by measuring the temperature dependence of zero-field cooled susceptibility without any intermittent stops. The results are shown in Fig. 4(c). The data are depicted as $M(T_s,T)/M_{MAX}(T_s)$, where $M_{MAX}(T_s)$ is the maximum value of $M(T_s,T)$.[37] In the vicinity of T_s, the $M(T_s,T)/M_{MAX}(T_s)$ becomes lower compared

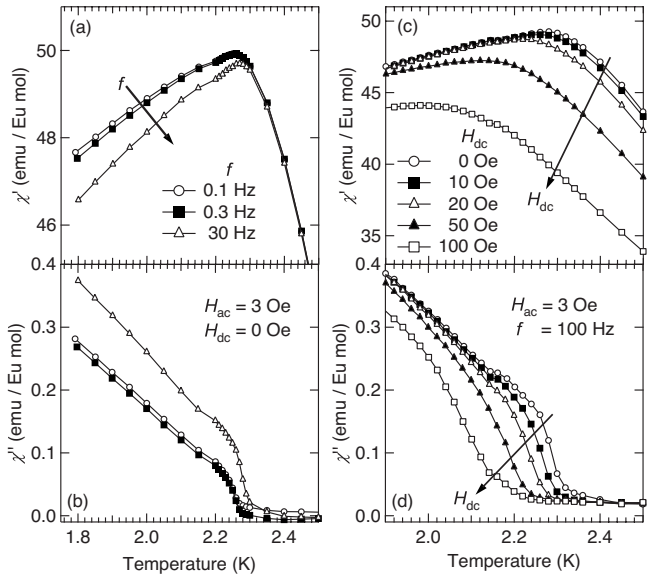

FIG. 5. Temperature dependence of ac susceptibility for $60.0EuO \cdot 11.0Al_2O_3 \cdot 19.5B_2O_3 \cdot 9.5SiO_2$ glass: (a) real part, $\chi'(T)$ and (b) imaginary part, $\chi''(T)$. Temperature dependence of ac susceptibility measured in a series of superimposed dc magnetic fields: (c) $\chi'(T)$ and (d) $\chi''(T)$.

to $M(\mathrm{ref},T)/M_{\mathrm{MAX}}(\mathrm{ref})$. The effect of aging at T_s is reflected by the dip at around T_s. The zero-field memory effect is characteristic of SG and related systems;[38] such a phenomenon has been never observed in a simple ferromagnet, so that the result shown in Fig. 4(c) strongly indicates that the present glass is a reentrant ferromagnet. Nonetheless, the SG transition temperature of the present glass can not be definitely determined by the memory effect measurements since the memory effect is observed for both the SG and FM phases of RSG.[34] As demonstrated by the temperature dependence of ac susceptibility mentioned below, the SG transition temperature is lower than the lowest temperature of magnetic measurement, i.e., 1.8 K, and can not be determined.

Figure 4(d) displays specific heat, C_p, as a function of temperature measured at zero magnetic field. The C_p curve manifests a pronounced peak ascribable to a three-dimensional magnetic ordering at around 2.2 K. A gradual increase in C_p below 9 K shows the emergence of magnetic contribution in addition to the phonon contribution, which is in good agreement with the deviation of $\chi^{-1}(T)$ from the Curie-Weiss law, i.e., the onset of short-range FM ordering [see the inset of Fig. 3(a)]. An upturn of C_p below 1.2 K stems from the nuclear contribution of Eu.[39] A nondivergent behavior in specific heat at the transition temperature has been observed for various RSG systems in contrast to conventional ferromagnets.[35,40]

To gain insight of the magnetic transition, we have measured the ac susceptibility ($\chi_{ac}=\chi'-i\chi''$) of $60.0EuO \cdot 11.0Al_2O_3 \cdot 19.5B_2O_3 \cdot 9.5SiO_2$ glass. Figures 5(a) and 5(b) show the temperature dependence of real and imaginary parts of ac susceptibility, $\chi'(T)$ and $\chi''(T)$, respectively. The amplitude of ac magnetic field H_{ac} was set at 3 Oe while the frequency f was varied from 0.1 to 30 Hz. The $\chi'(T)$ curves exhibit a broad hump with a maximum at a temperature between 2.2 and 2.3 K and a shoulder at a temperature between 2.0 and 2.1 K. The behavior is very similar to that observed for $Eu_{0.54}Sr_{0.46}S$, a typical crystalline RSG material.[40] Two similar anomalies can be also observed in the temperature dependence of $\chi''(T)$; on cooling, the $\chi''(T)$ curve exhibits a remarkable jump at a temperature between 2.2 and 2.3 K, and manifests a slight change in slope at around 2.1 K. The results clearly demonstrate that the present glass undergoes a two-step magnetic transition, i.e., the RSG transition. A jump in $\chi''(T)$ on higher-temperature side occurs at around the peak temperature of specific heat, indicating that the susceptibility rise is attributed to the PM-FM transition. On the other hand, in general, the temperature of spin freezing into SG phase is determined by an inflection point of $\chi''(T)$. No infection points, however, are observed down to 1.8 K in the rise in $\chi''(T)$ on lower-temperature side, implying that the SG freezing occurs at a temperature lower than 1.8 K. The variation in $T_f(f)$ with the frequency, $\Delta T_f(f)/[T_f(f)\Delta \log f]$, is 0.0029. This value is small compared to those obtained for canonical SGs such as CuMn (the value is 0.005) and AuFe (0.010), and smaller by one order of magnitude than those obtained for amorphous oxide SGs such as cobalt aluminosilicate glass (0.06).[1] Namely, the ac susceptibility for the present glass is less sensitive to the frequency of H_{ac} compared to conventional SGs.

To further confirm the RSG nature of the present glass, the temperature dependence of ac susceptibility was measured at $H_{ac}=3$ Oe, and a superimposing dc magnetic field, H_{dc}. The frequency of H_{ac} was 100 Hz, and H_{dc} was varied from 0 to 100 Oe. The $\chi'(T)$ and $\chi''(T)$ curves are shown in Figs. 5(c) and 5(d), respectively. By applying H_{dc}, the jump in $\chi''(T)$ on the higher-temperature side is extremely suppressed while the rise in $\chi''(T)$ on the lower-temperature side is only slightly suppressed. A similar behavior was observed in various RSG systems, where the application of H_{dc} obscures the anomalous changes in $\chi'(T)$ and $\chi''(T)$ near the PM-FM transition temperature whereas the anomalies of $\chi'(T)$ and $\chi''(T)$ near the FM-SG transition temperature are insensitive to H_{dc}.[41–43] Thus, the results illustrated in Figs. 5(c) and 5(d) strongly evidence the RSG nature of the present glass.

Based on the aforementioned results obtained for the present glass, the low-temperature magnetic behavior can be summarized as follows. On lowering the temperature the present glass undergoes a magnetic transition at around 2.2 K from PM to FM states, at which the nonequilibrium dynamic phenomenon unique to SG is observed. The SG phase is present as the magnetically ordered phase below 1.8 K. The RSG nature implies the presence of minor AFM interactions to induce the magnetic frustration although FM interactions are predominant as revealed by the positive values of θ_W (see Sec. IV A).

V. POSSIBLE MECHANISM OF THE FERROMAGNETIC INTERACTION

It is obvious from Fig. 3(b) that the positive exchange interactions are predominant in the Eu^{2+}-containing oxide

glasses irrespective of the glass composition, indicating that the tendency for magnetic interaction to be FM is a common property of the oxide glasses containing Eu^{2+} ions. The result seems quite unaccountable, considering that AFM interactions are predominant in oxide glasses containing a large number of Gd^{3+}(~10 mol %) the electronic configuration ($4f^7$) of which is the same as that of Eu^{2+}.[13,14] It should be recalled that the FM interactions have been found in a series of insulating and crystalline Eu^{2+}-based compounds such as Eu chalcogenides.[23,44–48] The mechanism behind the FM exchange in such Eu^{2+}-based crystalline materials has been discussed from both experimental and theoretical standpoints in terms of their specific electronic structure.[23,24,49,50] These FM exchange mechanisms provide us with a clue as to the origin of the FM interactions in oxide glasses. Here, let us consider the possible mechanism of FM interactions among Eu^{2+} in oxide glasses.

Kasuya[24] demonstrated that the exchange interactions are FM for both nearest-neighbor 90° and next-nearest-neighbor 180° Eu^{2+}-O^{2-}-Eu^{2+} configurations in EuO. The result derived theoretically is in good agreement with experiments. Since only the local configurations of Eu^{2+} and O^{2-} are taken into account in this model, the exchange mechanisms can be applied to oxide glasses. For the 90° configuration, the dominant exchange path is based on a $4f$ spin excited to $5d$ band where it has an exchange interaction with another $4f$ spin on the nearest neighboring Eu^{2+}. This exchange interaction is called an indirect exchange via Eu $5d$ band. In this indirect FM exchange, oxide ions do not play an important role and an intra-atomic electron transfer from $4f$ to $5d$ is involved. The effective exchange integral of this interaction is proportional to $J_{\mathrm{intra}}b^2/U_{fd}^2$, where J_{intra} is the intra-atomic exchange integral between Eu $4f$ and $5d$ states and b the transfer integral between neighboring Eu ions. In the case of the present Eu^{2+}-containing glasses, an increase in Eu^{2+} concentration results in a decrease in the excitation energy U_{fd} as mentioned above (see Sec. III B). Therefore, this indirect FM exchange becomes stronger with an increase in Eu^{2+} concentration, consistent with the nonlinear dependence of θ_{W} on Eu^{2+} concentration [see Fig. 3(b)]. For the 180° configuration, Kasuya proposed three superexchange paths: the KA mechanism, superexchange mechanism via the d-f exchange interaction and the cross term between the above two mechanisms. By calculating the effective exchange integrals for the three exchange paths, he demonstrated that the first and second paths lead to the AFM interactions while the last cross term the FM interaction. In the case of EuO, the cross term makes the largest contribution among the three exchange paths, so that the exchange interaction is FM for the 180° configuration as a whole. The cross-term mechanism is based on the third-order perturbation via complicated processes among O $2p$, Eu $5d$, and Eu $4f$ states,[24] and involves interatomic O($2p$)-Eu($4f$,$5d$) transfer. Although the quantitative expression of this exchange mechanism involves some parameters such as U_{fd} in an intricate way, the expression suggests that an increase in the covalency of Eu^{2+}-O bond enhances the exchange integral. So, this mechanism also can explain the nonlinear increase in θ_{W} with an increase in Eu^{2+} concentration in the case of the present Eu^{2+}-containing glasses. Thus, FM coupling among neighboring Eu^{2+} ions is possible for the two representative configurations: the 90° and 180° Eu^{2+}-O^{2-}-Eu^{2+} configurations. Therefore, we can suggest that FM interactions are predominant in Eu^{2+}-containing oxide glasses, in which the Eu^{2+}-O^{2-}-Eu^{2+} angle has a wide distribution involving 90° and 180°.

Here, it should be noted that if all the magnetic interactions among the Eu^{2+} ions were FM, the FM state should be a magnetic ground state even in a disordered lattice; namely, the RSG state would not appear below the FM transition temperature. As mentioned in Sec. IV B, the coexistence of minor AFM interactions and major FM ones is a key factor for the appearance of the RSG, and in the present case, it may be related to a distribution of Eu^{2+}-Eu^{2+} distance. It has been reported that in europium chalcogenides such as EuO, EuS, EuSe, and EuTe, an increase in the ionic radius of anion from O to Te brings about an increase in the Eu^{2+}-Eu^{2+} distance and weakens the exchange interactions of both the 90° and 180° configurations.[44,49] Especially for the 180° configuration, the sign of exchange interaction varies from positive to negative with the increase in the Eu^{2+}-Eu^{2+} distance due to switching of the most contributing exchange path.[24] In other words, the pairs of Eu^{2+} spins can favor the AFM coupling as well as the FM one, depending on the relative configurations of the Eu^{2+} pairs and O^{2-} ions. It is naturally anticipated that the random network structure in the present glasses leads to a wide distribution in the Eu^{2+}-Eu^{2+} distance, and thus, some arrangements of Eu^{2+} and O^{2-} ions favor AFM interactions, although most arrangements of Eu^{2+} and O^{2-} ions prefer the FM interactions. Consequently, the present oxide glasses have a wide distribution in the sign of exchange interactions as well as their strength, which could trigger the observed RSG transition. At present, only qualitative explanation about the origin of FM interaction is possible due to the lack of detailed structural information of the present glasses such as the distributions of Eu^{2+}-Eu^{2+} distance and Eu^{2+}-O^{2-}-Eu^{2+} angle. The experimental techniques such as x-ray absorption fine structure will be useful for the structural analysis on the present glasses, which may allow quantitative discussion about the magnetic interactions including the demonstration of the presence of minor AFM interactions. Further extensive studies, especially on amorphous oxides with much higher Eu^{2+} concentrations, are required to corroborate the nature of magnetic transition as well as the mechanism of magnetic interactions.

VI. CONCLUSION

In conclusion, our experimental results reveal the dominance of FM interactions and the RSG behavior in the Eu^{2+}-based bulk oxide glasses, in contrast to most oxide glasses with predominant AFM interactions which lead to PM-SG transition. The FM interactions are preponderant among Eu^{2+} ions in all of the glasses examined in this study. In particular, $60.0EuO\cdot11.0Al_2O_3\cdot19.5B_2O_3\cdot9.5SiO_2$ glass definitely exhibits FM-PM transition at 2.2 K. The discussion about the origin of the FM interaction on the basis of the FM exchange mechanism suggested for Eu^{2+}-based crystalline compounds leads to the conclusion that the exchange coupling attributed to the unique electronic state of Eu^{2+} ion can

work as FM interactions for any Eu^{2+}-O^{2-}-Eu^{2+} bond angles. The disordered glass structure allows the local configuration of Eu^{2+}-O^{2-}-Eu^{2+} which gives rise to AFM interaction, leading to the RSG transition.

ACKNOWLEDGMENTS

The authors thank M. Tosaki and Y. Isozumi of Radioisotope Research Center, Kyoto University, for the Mössbauer effect measurements and M. Azuma and Y. Shimakawa of Institute for Chemical Research, Kyoto University, for the specific-heat measurements. This research was partially supported by the Ministry of Education, Science, Sports and Culture, Grant-in-Aid for Scientific Research (B) (Grant No. 19360298) and Challenging Exploratory Research (Grant No. 21656163). One of the authors (H.A.) thanks the Grant-in-Aid (Grant No. 20-6726) from Japan Society for the Promotion of Science (JSPS).

*Corresponding author; fujita@dipole7.kuic.kyoto-u.ac.jp

[1] J. A. Mydosh, *Spin Glasses: An Experimental Introduction* (Taylor & Francis, London, 1993).
[2] H. A. Kramers, Physica (Amsterdam) **1**, 182 (1934).
[3] P. W. Anderson, Phys. Rev. **79**, 350 (1950).
[4] J. B. Goodenough, Phys. Rev. **100**, 564 (1955).
[5] J. Kanamori, J. Phys. Chem. Solids **10**, 87 (1959).
[6] H. Akamatsu, K. Fujita, S. Murai, and K. Tanaka, Appl. Phys. Lett. **92**, 251908 (2008).
[7] J. P. Sanchez, J. M. Friedt, R. Horne, and A. J. van Duyneveldt, J. Phys. C **17**, 127 (1984).
[8] R. A. Verhelst, R. W. Kline, A. M. de Graaf, and H. O. Hooper, Phys. Rev. B **11**, 4427 (1975).
[9] K. Tanaka, H. Akamatsu, S. Nakashima, and K. Fujita, J. Non-Cryst. Solids **354**, 1347 (2008).
[10] H. Akamatsu, K. Tanaka, K. Fujita, and S. Murai, J. Phys.: Condens. Matter **20**, 235216 (2008).
[11] H. Akamatsu, S. Oku, K. Fujita, S. Murai, and K. Tanaka, Phys. Rev. B **80**, 134408 (2009).
[12] H. Akamatsu, S. Murai, K. Fujita, and K. Tanaka, Adv. Mater. Res. **39-40**, 207 (2008).
[13] I. Ardelean and L. Griguta, J. Non-Cryst. Solids **353**, 2363 (2007).
[14] S. Simon, R. Pop, V. Simon, and M. Coldea, J. Non-Cryst. Solids **331**, 1 (2003).
[15] P. Beauvillain, C. Dupas, J. P. Renard, and P. Veillet, Phys. Rev. B **29**, 4086 (1984).
[16] H. Akamatsu, K. Tanaka, K. Fujita, and S. Murai, Phys. Rev. B **74**, 012411 (2006).
[17] H. Akamatsu, K. Tanaka, K. Fujita, and S. Murai, J. Magn. Magn. Mater. **310**, 1506 (2007).
[18] F. J. Litterst, J. Phys. (France) Lett. **36**, 197 (1975).
[19] J. Schoenes, E. Kaldis, W. Thöni, and P. Wachter, Phys. Status Solidi A **51**, 173 (1979).
[20] S. Foner, Proceedings of the International Conference on Magnetism, Nottingham, London, 1964 (Institute of Physics and the Physical Society, London, 1964), p. 438.
[21] G. K. Wertheim and D. N. E. Buchanan, Phys. Rev. **161**, 478 (1967).
[22] Y. Sugihara, T. Hayakawa, and M. Nogami, J. Ceram. Soc. Jpn. **115**, 602 (2007).
[23] C. L. Chien, S. Debenedetti, and F. D. S. Barros, Phys. Rev. B **10**, 3913 (1974).
[24] T. Kasuya, IBM J. Res. Dev. **14**, 214 (1970).
[25] K. Fujita, K. Tanaka, K. Hirao, and N. Soga, J. Am. Ceram. Soc. **81**, 1845 (1998).
[26] It is believed that the recoil-free fraction is smaller for Eu^{2+} ion than for Eu^{3+} ion in oxide glasses due to the difference in the valence state and ionic radius between Eu^{2+} and Eu^{3+} when Coulomb force is only taken into account. Actually, the recoil-free fraction for Eu^{2+} is smaller than for Eu^{3+} in fluorozirconate glasses as estimated by J. M. D. Coey, A. McEvoy, and M. W. Shafer, J. Non-Cryst. Solids **43**, 387 (1981).
[27] G. H. Shenoy and B. D. Dunlap, Nucl. Instrum. Methods **71**, 285 (1969).
[28] K. Tanaka, K. Fujita, N. Soga, J. Qiu, and K. Hirao, J. Appl. Phys. **82**, 840 (1997).
[29] K. Tanaka, K. Fujita, N. Matsuoka, K. Hirao, and N. Soga, J. Mater. Res. **13**, 1989 (1998).
[30] J. H. Van Vleck, *The Theory of Electric and Magnetic Susceptibility* (Clarendon, Oxford, 1932).
[31] K. Koteswara Rao, M. Vithal, and D. Ravinder, J. Magn. Magn. Mater. **253**, 65 (2002).
[32] K. Kugimiya, K. Fujita, K. Tanaka, and H. Hirao, J. Magn. Magn. Mater. **310**, 2268 (2007).
[33] K. Fujita, N. Wakasugi, S. Murai, Y. Zong, and K. Tanaka, Appl. Phys. Lett. **94**, 062512 (2009).
[34] V. Dupuis, E. Vincent, M. Alba, and J. Hammann, Eur. Phys. J. B **29**, 19 (2002).
[35] A. A. Belik, N. Tsuji, Q. Huang, E. Takayama-Muromachi, and M. Takano, J. Phys.: Condens. Matter **19**, 145221 (2007).
[36] R. Mathieu, P. Jönsson, D. N. H. Nam, and P. Nordblad, Phys. Rev. B **63**, 092401 (2001).
[37] The magnetic behavior of the present system is very sensitive to magnetic field. We selected such a low magnetic field of 1 Oe as a measuring field since the magnetic field higher than 10 Oe made the memory effect too obscure to be observed. Due to the low accuracy of 1 Oe, the data are presented as a normalized magnetization, i.e., $M(T_s,T)/M_{MAX}(T_s)$.
[38] M. Sasaki, P. E. Jönsson, H. Takayama, and H. Mamiya, Phys. Rev. B **71**, 104405 (2005).
[39] O. W. Dietrich, A. J. Henderson, and H. Meyer, Phys. Rev. B **12**, 2844 (1975).
[40] D. Meschede, F. Steglich, W. Felsch, H. Maletta, and W. Zinn, Phys. Rev. Lett. **44**, 102 (1980).
[41] H. Maletta and W. Felsch, Z. Phys. B **37**, 55 (1980).
[42] K. Jonason, J. Mattsson, and P. Nordblad, Phys. Rev. B **53**, 6507 (1996).
[43] Y. Yeshurun, M. B. Salamon, K. V. Rao, and H. S. Chen, Phys. Rev. B **24**, 1536 (1981).
[44] T. R. McGuire and M. W. Shafer, J. Appl. Phys. **35**, 984 (1964).
[45] B. T. Matthias, R. M. Bozorth, and J. H. Van Vleck, Phys. Rev.

Lett. **7**, 160 (1961).
[46] M. W. Shafer, J. Appl. Phys. **36**, 1145 (1965).
[47] J. E. Greedan and G. J. McCarthy, Mater. Res. Bull. **7**, 531 (1972).
[48] H. Hata, G. Adachi, and J. Shiokawa, Mater. Res. Bull. **12**, 811 (1977).
[49] N. M. Souza-Neto, D. Haskel, Y. C. Tseng, and G. Lapertot, Phys. Rev. Lett. **102**, 057206 (2009).
[50] R. Ranjan, H. S. Nabi, and R. Pentcheva, J. Appl. Phys. **105**, 053905 (2009).